Fibroblasts regulate lymphatic barrier functions in a tissue-dependent manner

Sarfaraz Ahmad Ejazi[1], Aisha Abdulkarimu[1], Theodore Hsiao[1], Rony Garcia-Vivas[1], Katharina Maisel[1*]

Affiliations:

1: Fischell Department of Bioengineering, University of Maryland, College Park

*** Correspondence to:**

Dr. Katharina Maisel

Fischell Department of Bioengineering

University of Maryland, College Park USA

Email: maiselka@umd.edu

ABSTRACT

The lymphatic vasculature plays a vital role in clearing interstitial fluid from tissues and guiding immune cell transport. Junctions between lymphatic endothelial cells (LECs) are important for preserving vascular integrity. Tight junction proteins like ZO-1 work alongside adherens proteins such as VE-cadherin to regulate barrier function and vascular permeability. Fibroblasts contribute to the lymphatic interstitial environment by producing extracellular matrix components and affecting lymphatic functions and lymphangiogenesis. Despite their known roles, the direct impact of fibroblasts on LEC barrier function remains poorly understood. Here, we established a non-contact in vitro co-culture system to investigate how fibroblasts influence LEC junctions and permeability.

We began by assessing the effect of secreted factors (secretomes) from normal human dermal fibroblasts (NHDFs) on human LECs (hLECs) that led to a 126% increase in the transendothelial electrical resistance (TEER) of the hLEC monolayer.

Immunofluorescence analysis revealed a >4-fold increase in the junctional expression of ZO-1 and VE-cadherin, with no changes observed in PROX-1 and LYVE-1, key lymphatic markers. Additionally, transport of FITC- dextran across hLECs reduces by 24% upon NHDF secretome treatment. Co-culture of hLECs with growth factor-activated, NHDF(G) and -inactivated, NHDF(B) fibroblasts increase TEER by 143% and 106%, respectively, indicating improved monolayer integrity. Confocal microscopy revealed that ZO-1 expression increased by 2.1- and 2.0-fold, and VE-cadherin levels rose by 1.6- and 1.3-fold in the NHDF(G) and NHDF(B) groups, compared to untreated controls. Dextran permeability dropped by 30% with NHDF(G) and 15% with NHDF(B), confirming reduced permeability. A junction analyzer program (JAnaP) showed a rise in continuous ZO-1 junctions from 84% in controls to over 96% in NHDF co-cultures. Besides, NHDFs significantly reduced discontinuous junctions, with a decrease in punctate junctions by 89% and 97% and perpendicular junctions by 64% and 62% with NHDF(G) and NHDF(B), respectively. Surprisingly, we found an opposite effect with normal human lung fibroblast (NHLF) secretome on hLEC junctional integrity and permeability. NHLFs significantly lowered TEER, along with ZO-1 expression, and doubled dextran permeability across the hLEC monolayer. Treatment of hLECs with thrombin, a potent inflammatory mediator, led to impaired cell junctions, more profoundly in the presence of NHDFs.

The RNA-seq data showed upregulation of key lymphatic markers in fibroblast-induced hLECs such as LYVE-1, FOXC2, junctional genes CLDN5 and GJA4, and actin-related genes including ACTG1, RACK1, and RHOG, suggesting potential modulation of junctional integrity and cytoskeletal organization. In contrast, genes associated with endothelial adhesion to surrounding cells and extracellular matrix, such as ICAM1, VCAM1, ITGB1, ITGA, and SELE were downregulated, indicating reduced cell–cell and cell–matrix interactions. Fibroblast co-culture also enhanced the expression of genes involved in endothelial-to-mesenchymal transition (EndoMT) and increased levels of ECM-degrading metalloproteinases, potentially impairing ECM–LEC interactions. Gene Ontology (GO) enrichment analysis of the differentially expressed genes highlighted significant changes in biological pathways related to cell adhesion, ECM

remodeling, inflammatory responses, transcriptional regulation, signal transduction, and angiogenesis.

This study highlights the role of fibroblasts in regulating lymphatic barrier function by modulating endothelial cell-cell junctions. Notably, their impact on LECs varies based on fibroblast tissue origin, revealing functional heterogeneity. These findings offer valuable insights for developing targeted lymphatic delivery strategies to modulate lymphatic functions and improve therapeutic outcomes, including vaccine performance.

INTRODUCTION

Lymphatic vessels are found throughout the entire body and are responsible for transporting immune cells, regulating fluid homeostasis, and absorbing dietary fats. Dysfunction of the lymphatic vasculature can contribute to a range of pathological conditions, including lymphedema, chronic inflammation, and cancer progression. Lymphatic vessels are lined with lymphatic endothelial cells (LECs) with distinct morphological and functional arrangements. The initial (or capillary) lymphatics are lined with LECs, loosely connected with discontinuous (button-like) junctions and a discontinuous basement membrane with no perivascular cells. Fluid, antigens, cells, and debris are transported into initial lymphatics from the peripheral tissues, and upon collection into the initial vessel lumen, the lymph fluid is shuttled into pre-collectors and eventually larger collecting vessels. Collecting lymphatics are lined with LECs connected with continuous, tight (zipper-like) cell-cell junctions and have a complete basement membrane surrounded by smooth muscle cells (SMCs) and perivascular cells. The paired leaflet valves and phasic contraction of SMCs facilitate the directional lymph flow in the collecting lymphatics and toward the thoracic ducts.

Two junction types, tight and adherens junctions, regulate lymphatic integrity and permeability, and are arranged in either button- or zipper-like fashion in initial and collecting vessels, respectively. Studies have highlighted the role of adherens junction proteins, including VE-cadherin, in supporting button-like junctions of initial lymphatics. A decrease in VE-cadherin expression may enhance lymphatic vessel permeability and allow immune cells to migrate into lymphatic vessels [1,2]. Tight junction proteins such

as claudin-5 and zonula occludins (ZO) regulate paracellular permeability by forming an intercellular barrier to control the movement of proteins, molecules, and ions across the LECs. ZO-1 interacts with tight junction proteins and actin filaments to maintain LEC junctional integrity. Expression of claudin-5 and ZO-1 was found to be downregulated in inflammation, suggesting changes in lymphatic vessel permeability [3]. Alterations in expression or function of these proteins have been linked to several pathological conditions related to lymphatic dysfunction, including edema, inflammation, and cancer metastasis [4]. Indeed, many factors including inflammatory cytokines, vascular endothelial growth factor (VEGF-C), and mechanical forces like fluid shear stress and interstitial pressure, can affect the integrity of LEC junctions and lymphatic vessel permeability [5-7]

Advancements in lymphatic vascular biology revealed the complex interplay between LECs and other cell types, and researchers have attempted to identify cells and molecular signals that affect lymphatic permeability [8]. In the interstitium, lymphatic vessels are surrounded by various extracellular matrix (ECM) proteins and residing immune cells and fibroblasts. Fibroblasts secrete ECM proteins, such as collagen, and can directly modulate the mechanical environment adjacent to lymphatic vessels. Fibroblasts have also been shown to secrete VEGF-C, which is known to regulate lymphangiogenesis by promoting vascular sprouting, tube formation, and vessel integrity through stimulating VEGFR3-mediated MAPK/ERK and AKT intracellular pathways [9-12]. The role of fibroblast growth factor (FGF) signaling in lymphangiogenesis was also demonstrated, as vessel sprouting was inhibited following the knockdown of FGFR1 in dermal LECs [13].

In the context of lymphatic vessels, fibroblasts have been studied in several physiological and pathological conditions, such as cancer and wound healing. For example, cancer-associated fibroblasts contribute to metastasis by inducing lymphangiogenesis and promoting lymphatic permeability within the tumor microenvironment by downregulating VE-cadherin [14]. Additionally, tumor-derived fibroblasts from head and neck cancer increased lymphatic vessel sprouting and altered in lymphatic permeability [15]. Fibroblasts have also been implicated in the repair and regeneration of lymphatic vessels during wound healing. An in vitro engineered

lymphatic model demonstrated fibroblast matrix guided lymphangiogenesis in wound healing [16].

To investigate the complex crosstalk of lymphatic endothelial cells in a physiologically relevant matrix along with living fibroblasts, a co-culture system has been utilized in many studies. Most of the recent studies on the influence of LECs in response to fibroblasts have focused on lymphangiogenesis or immune and cancer cell trafficking, mainly in the context of disease. However, the homeostatic effects of fibroblast cells on lymphatic barrier function and integrity are not well understood. Here, we developed a non-contact in vitro co-culture model to examine fibroblast regulation of lymphatic cell-cell junctions, barrier integrity, and permeability. We first studied the response of human LECs (hLECs) to secreted factors from normal human dermal fibroblasts (NHDFs) on LEC junction integrity and permeability and found tissue-specific differences. We further studied fibroblasts/LEC co-cultures on collagen beds, where NHDFs appeared to support hLEC junction integrity and reduced paracellular transport. RNA sequence analysis supported these findings and revealed the upregulation of genes responsible for both hLEC morphology and the cytoskeletal framework necessary for barrier function. Our study highlights the effect of fibroblasts on lymphatic functions during homeostasis, critical to understanding potential mechanistic targets that could allow lymphatic functions to return to homeostasis during disease.

RESULTS

Exposure to fibroblast secretomes modulates lymphatic cell-cell junctions and reduces lymphatic permeability.

To understand the effect of fibroblasts on hLEC junction, we first optimized the media conditions for fibroblast secretome collection. We found that the characteristic morphology and growth pattern of NHDF cells were similar in endothelial microvascular growth media (EGMV2), as this media also contains fibroblast growth factors. NHDFs were grown in either fibroblast growth media (FGM) with 1ng/mL of fibroblast growth factor and 5 µg/mL of insulin [NHDF(G)], or in basal FGM [NHDF(B)]. Then, NHDFs were exposed to EGMV2 low serum media for a day and NHDF secretome was

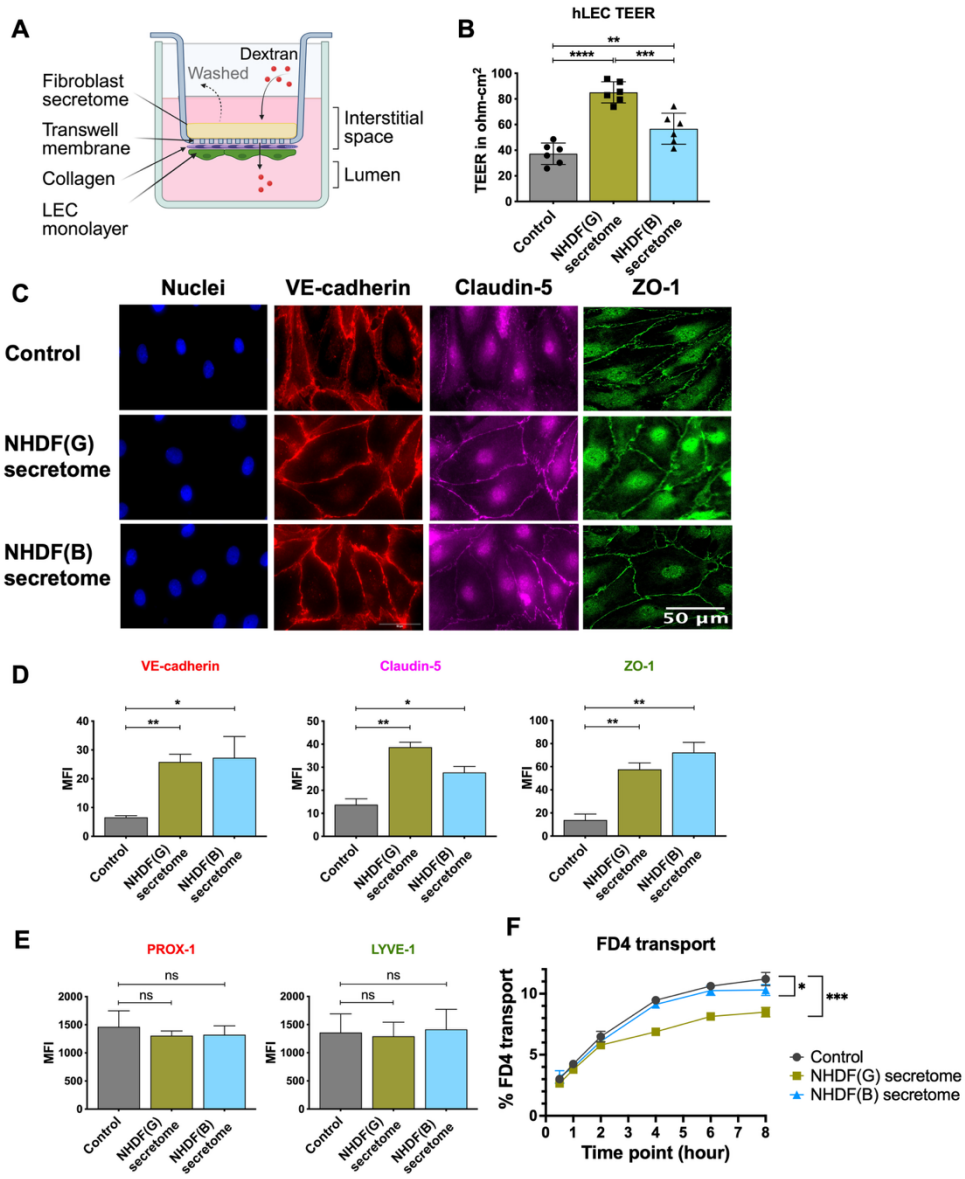

Figure 1. ***NHDF secretomes increase hLEC barrier functions.*** **(A)** Schematic diagram of transwell secretome experiment. (**B)** TEER measurements of hLEC monolayers after 48 hours of treatment with dermal fibroblast secretomes from NHDF(G) and NHDF(B). (**C)** Representative immunofluorescence images of VE-cadherin, claudin-5, and ZO-1 on hLECs following treatment with NHDF secretomes. **(D)** Quantification of VE-cadherin, claudin-5, and ZO-1 expression levels using ImageJ (FIJI). **(E)** Quantification of lymphatic markers LYVE-1 and PROX1 expression in hLEC monolayers treated with NHDF secretomes. **(F)** FITC–Dextran (4 kDa) transport assay across hLECs after NHDF secretome treatment. Data are presented as mean ± SEM from n = 6 independent experiments. Statistical analysis was performed using an unpaired two-tailed t-test; $p > 0.05$ = not significant (ns), $p \leq 0.0001$ = extremely

significant (****). For the permeability (transport) assay (n = 3, representative), statistical significance was determined by two-way ANOVA followed by appropriate post hoc test for multiple comparisons.

collected. hLECs were grown in a monolayer on a transwell insert and then treated with NHDF(G) or (B) secretomes for 2 days (**Figure 1A**). We first assessed hLEC barrier integrity using transendothelial electrical resistance (TEER). Treatment with NHDF(G) and NHDF(B) secretomes resulted in significantly higher TEER values of 85 ± 8 Ω-cm^2 and 57 ± 12 Ω-cm^2, respectively, compared to 37 ± 8 Ω-cm^2 for the controls (**Figure 1B**). Next, we sought to analyze hLEC cell-cell junction integrity and expression via immunofluorescence. We found that tight junction proteins (ZO-1 and claudin-5) and adherens junction protein (VE-cadherin) expression significantly increased with both the NHDF secretomes compared to controls (**Figure 1C&D**). Specifically, treatment with NHDF(G) led to 4-, 3-, and 4-fold increases in the expression levels of VE-cadherin, claudin-5, and ZO-1, respectively, while NHDF(B) treatment resulted in 4-, 2-, and 5-fold upregulation of the junction proteins, respectively (**Figure 1D**). We also found that lymphatic endothelial markers, LYVE-1 and PROX1, were not altered (**Figure 1E & Supplementary figure 1A**). To evaluate changes in hLEC monolayer permeability following treatment with fibroblast secretomes, we assessed transport of a fluorescently labeled, 4kDa dextran (FD4). We observed a 24% reduction in permeability, decreasing from 11 ± 1% in the control group to 8 ± 1% with NHDF(G) secretome-treated group after 8 hours (**Figure 1F**).

Co-culture with fibroblasts regulates LEC junction expression and reduces lymphatic permeability

To address the direct effects of fibroblasts on the lymphatic junction expression and permeability, we generated a non-contact co-culture model (**Figure 2A**), where hLECs are cultured on the bottom of the transwell and after monolayers were established, NHDFs were seeded on the transwell top. Cells were co-cultured for 2 days (**Figure 2A**), after which fibroblasts were scraped from the membrane to prevent interference

with TEER and permeability measurements. hLEC monolayers exhibited increased TEER values after co-culture with NHDF(G) and (B), rising from 46 ± 13 for the control group to 112 ± 5 with NHDF(G) and 95 ± 15 with NHDF(B) treatments (**Figure 2B**). We also found a distinct increase in ZO-1 and VE-cadherin expression in both co-culture groups (**Figure 2C**). VE-cadherin expression increased by 1.6- and 1.3-fold, while ZO-1

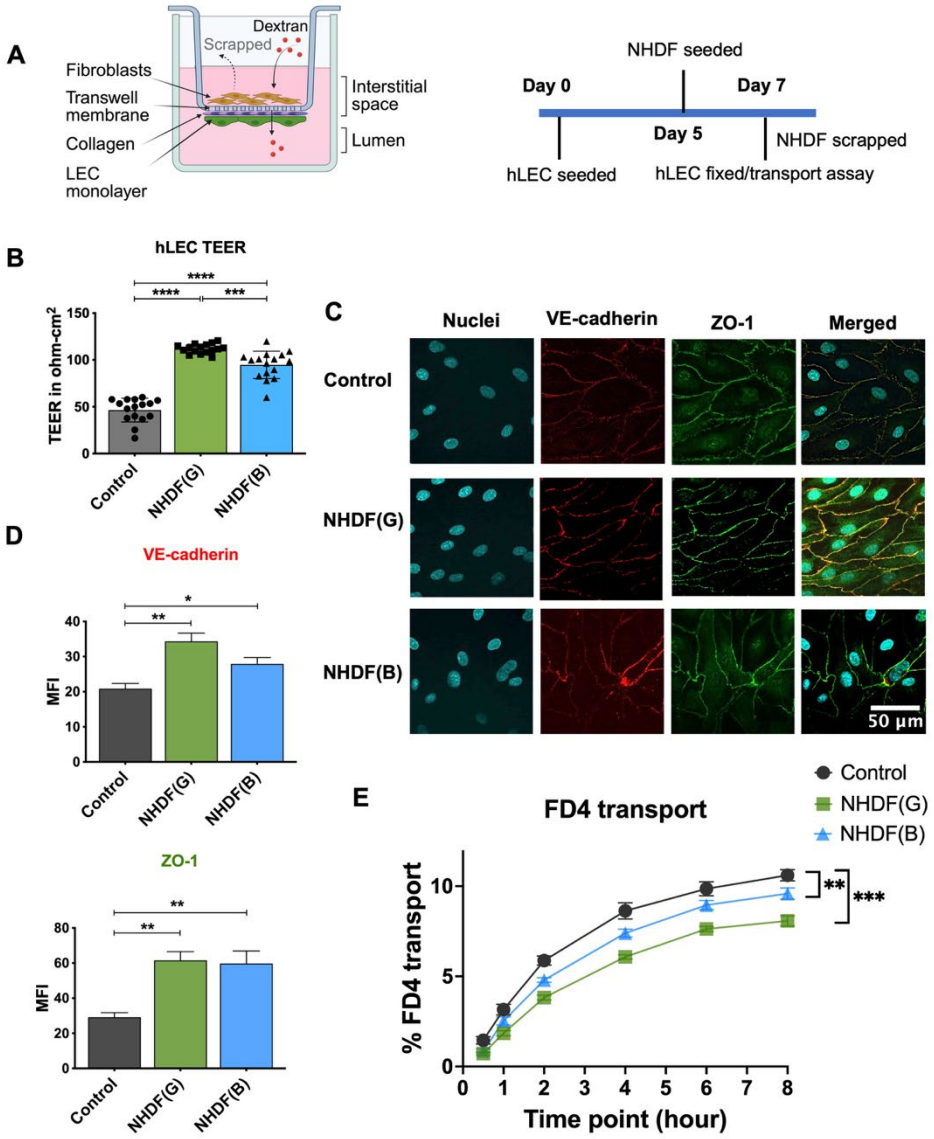

Figure 2. ***NHDF co-culture with hLECs increases hLEC barrier functions.*** **(A)** Schematic diagram of transwell co-culture experiment and timeline of cell seedings and

co-culture. **(B)** TEER measurements of hLEC monolayers after 48 hours of co-culture with dermal fibroblasts, NHDF(G) and NHDF(B). **(C)** Representative immunofluorescence images of VE-cadherin, and ZO-1 on hLECs following co-culture with NHDFs. **(D)** Quantification of VE-cadherin and ZO-1 expression levels using ImageJ (FIJI). **(E)** FITC–Dextran (4 kDa) transport assay across hLECs after co-culture with NHDFs. Data are presented as mean ± SEM from $n = 6$ independent experiments. Statistical analysis was performed using an unpaired two-tailed *t*-test; $p > 0.05$ = not significant (ns), $p \leq 0.0001$ = extremely significant (****). For the permeability (transport) assay ($n = 9$, representative), statistical significance was determined by two-way ANOVA followed by appropriate post hoc test for multiple comparisons.

expression increased by 2.1- and 2.0-fold in the NHDF(G) and NHDF(B) groups, respectively, compared to the control group (**Figure 2D**). FD4 permeability across the hLEC monolayer decreased by 24% following co-culture with NHDF(G), and by 9.5% with NHDF(B), indicating reduced permeability (**Figure 2E)**.

We performed detailed analysis of LEC junction morphology using the Junction Analyzer Program (JAnaP) [17], a Python-based program that quantitatively analyzes cell-cell junction presentation along with cell morphology. We found no difference in the cellular solidity, but did see an 18% decrease in the cell circularity of hLECs co-cultured with NHDF(G) (**Figure 3A**). Both NHDF(G) and (B) promote lymphatic monolayers, increasing hLEC coverage by 7%. We also found a significant increase in ZO-1 continuous junctions from 84 ± 5% in controls to 96 ± 2% in both co-cultures. Similarly, both co-cultures significantly reduced ZO1 discontinuous junctions, with reductions in punctate junctions by 89% and 97% and perpendicular junctions by 64% and 62% with NHDF(G) and NHDF(B), respectively (**Figure 3A**). Immunoblot analysis showed no notable increase in overall ZO-1 (220 kDa) and VE-cadherin (120 kDa) protein levels compared to the control (**Figure 3B**). Similarly, mRNA expression levels of ZO-1 and VE-cadherin (**Figure 3C**), along with lymphatic markers, PROX-1 and LYVE-1 (**Supplementary figure 1B**) did not differ significantly from the control.

Fibroblasts show tissue-specific effects on lymphatic junctions and permeability.

To investigate tissue-specific effects of fibroblasts on lymphatic functions, we exposed hLECs to secretome from normal human lung fibroblasts (NHLF). While we found a significant increase in junction integrity and TEER with dermal fibroblast (NHDF)

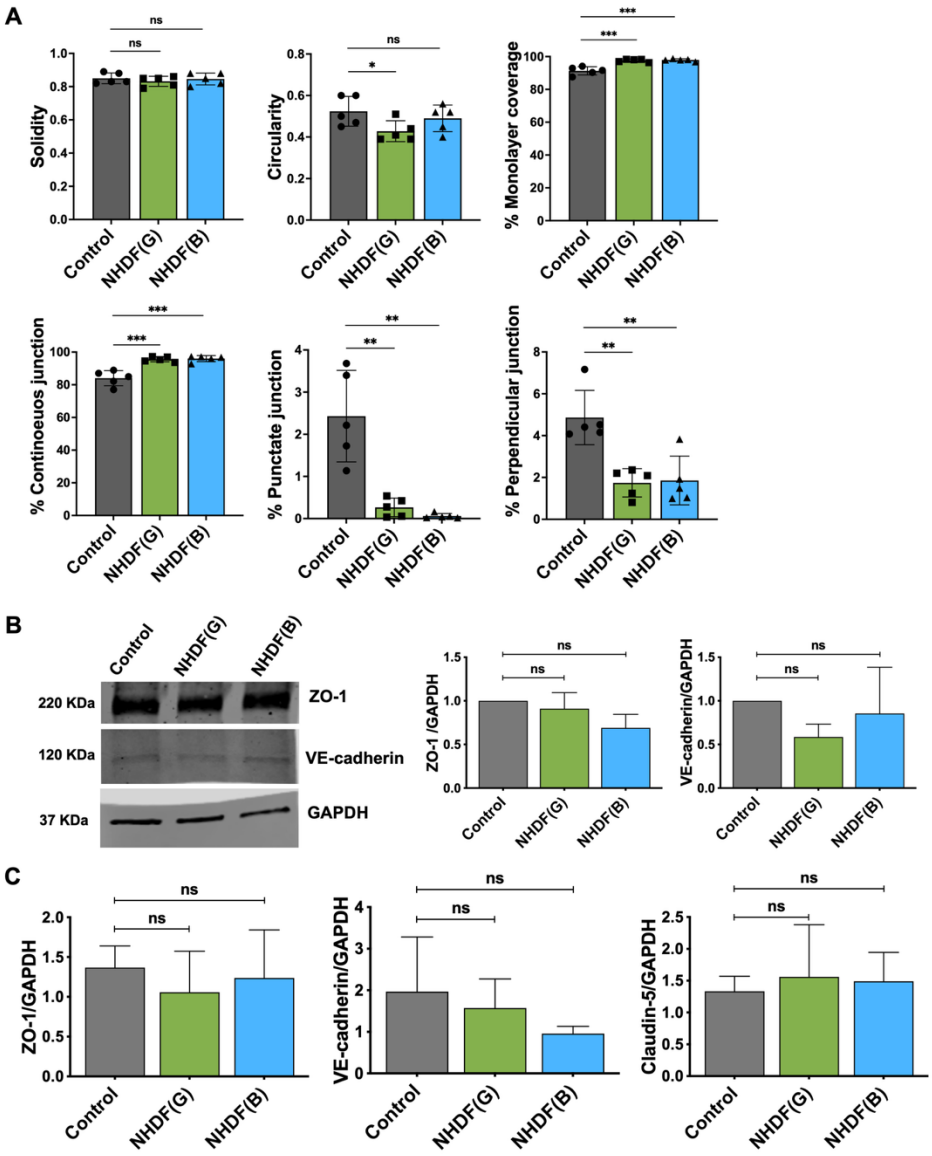

Figure 3. ***hLEC junctions are tightened after co-culture with NHDFs.*** **(A)** Quantitative analysis of ZO-1 distribution and organization in hLEC monolayers using JAnaP after 48 hours of co-culture with NHDFs. **(B)** Immunoblot analysis of total ZO-1 (220 kDa) and VE-cadherin (120 kDa) protein expression levels in hLECs following co-culture. **(C)** RT-qPCR analysis of mRNA expression levels of ZO-1 and VE-cadherin in hLECs under the same conditions. Data are presented as mean ± SEM from $n > 2$

independent experiments. Statistical analysis was performed using an unpaired two-tailed *t*-test; $p > 0.05$ = not significant (ns), $p \leq 0.0001$ = extremely significant (****).

secretomes, we detected the opposite trend with NHLFs. There was a significant decrease in TEER from 87 ± 5 Ω-cm^2 in the control to 72 ± 2 Ω-cm^2 with NHLF secretomes (**Figure 4A**). Immunofluorescence imaging revealed an 18% reduction in ZO-1 expression following treatment with NHLF secretome, compared to the control, while treatment with NHLF media left expression unchanged. (**Figure 4B&C**). We found no significant change in VE-cadherin expression compared to the control. Consistent with the reduction in TEER and ZO-1 expression, we observed a 2-fold increase in FD4 transport across hLECs treated with NHLF secretome compared to controls. We also saw that this effect was dose-dependent, as the FD4 transport increases with an increase in secretome proportion (**Figure 4D**).

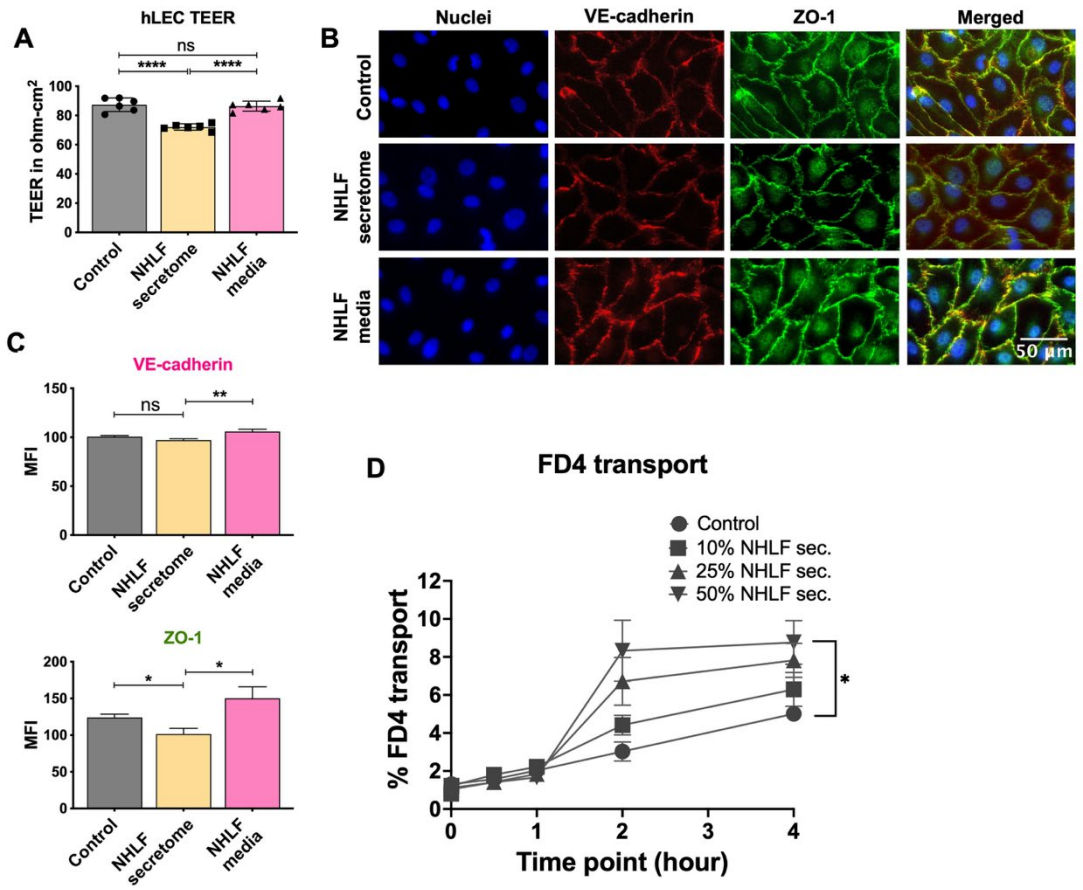

Figure 4. ***NHLF secretomes reduce hLEC barrier functions.*** **(A)** TEER measurements of hLEC monolayers after 48 hours of treatment with NHLF secretomes or fibroblast media. **(B)** Representative immunofluorescence images of VE-cadherin, and ZO-1 on hLECs following treatment with NHLF secretome. **(C)** Quantification of VE-cadherin and ZO-1 expression levels using ImageJ (FIJI). **(D)** FITC–Dextran (4 kDa) transport assay across hLECs after treatment with 10, 25, and 50% NHLF secretome. Data are presented as mean ± SEM from $n = 6$ independent experiments. Statistical analysis was performed using an unpaired two-tailed *t*-test; $p > 0.05$ = not significant (ns), $p \leq 0.0001$ = extremely significant (****). For the transport assay ($n = 3$, representative), statistical significance was determined by two-way ANOVA followed by appropriate post hoc test for multiple comparisons.

Fibroblasts promote thrombin-induced LEC barrier dysfunction

Thrombin, a potent inflammatory mediator, is known to induce vascular dysfunction and increase endothelial permeability in blood vasculature. However, the effects of thrombin signaling on lymphatic function, particularly its impact on permeability, remain to be fully understood. Studies on HUVECs have shown that thrombin disrupts endothelial integrity by altering VE-cadherin and catenin interactions [18]. We examined the impact of thrombin on hLECs in the presence of fibroblasts. hLECs were either exposed to thrombin for 4 hours or left untreated, followed by a 48-hour co-culture with NHDF, with an hLEC-only group serving as a control. Thrombin treatment caused a reduction in TEER values in hLECs by 19%, while a 12% decrease was observed in the NHDF co-culture group (**Figure 5A**). Thrombin treatment also led to a reduction in hLEC numbers for both control and NHDF groups, suggesting a potential impact on cell viability or proliferation (**Figure 5B**). Additionally, we assessed the permeability of hLECs to FD4 after thrombin treatment in response to NHDF co-culture. Consistent with the TEER findings, thrombin increased dextran transport by 30% in hLECs in the presence of fibroblasts (**Figure 5C**). Immunofluorescence analysis of junction proteins in thrombin-treated hLECs showed an irregular junction protein expression between the cell-cell

monolayer. When hLECs were co-cultured with NHDF after thrombin treatment, they exhibited noticeably larger junction discontinuity (**Figure 5D**).

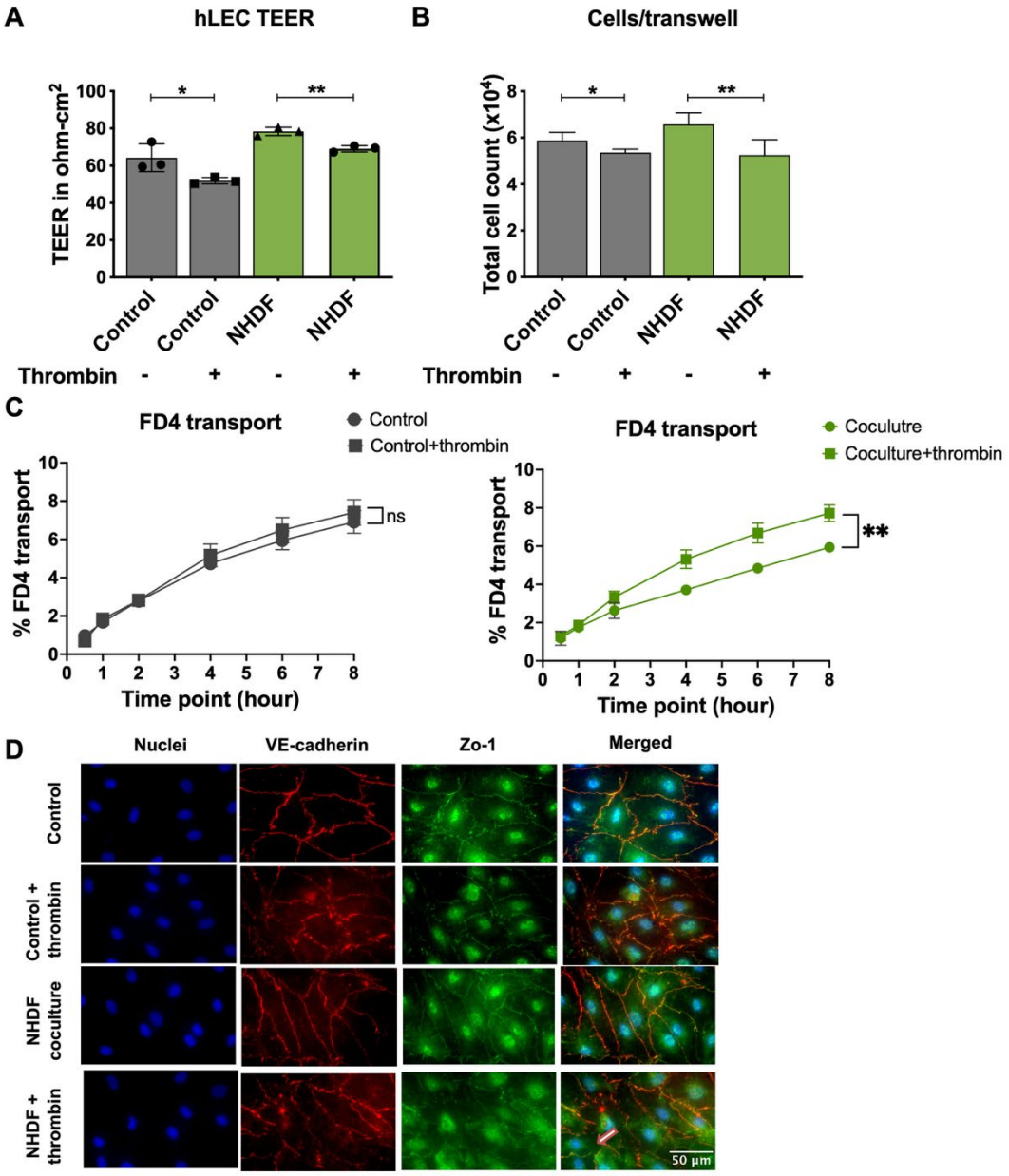

Figure 5. ***Thrombin modulates hLEC barrier integrity only in the context of co-culture with NHDFs.*** **(A)** TEER measurements of hLEC monolayers after 4 hours of thrombin treatment followed by 48 hours of co-culture with dermal fibroblast, NHDF(G) (*n = 3*). **(B)** Total cell counts (*n = 6*). **(C)** FITC–Dextran (4 kDa) transport assay across hLECs after 4 hours of thrombin stimulation and/or NHDF(G) co-culture for 48 hours.

(D) Representative immunofluorescence images of ZO-1 and VE-cadherin on hLECs with and without thrombin treatment. Data are presented as mean ± SEM from *n = 3-6* independent experiments. Statistical analysis was performed using an unpaired two-tailed *t*-test; $p > 0.05$ = not significant (ns), $p \leq 0.0001$ = extremely significant (****). For the transport assay, statistical significance was determined by two-way ANOVA followed by appropriate post hoc test for multiple comparisons.

RNA-seq reveals fibroblast treatment of hLECs modulates gene expression related to ECM, cell-cell adhesion, and junctions

We next sought to investigate the transcriptomic impact of fibroblasts on LECs. We performed RNA-seq analysis of hLECs following co-culture with NHDF(G) and NHDF(B) to obtain the differentially expressed genes (DEGs). The NHDF(G)-induced hLEC data revealed 2,211 genes were upregulated and 1,744 were downregulated (**Figure 6A&6B**). Notably, the expression of key lymphatic markers, including LYVE-1, FOXC2, and PROX1, and upstream regulators SOX18 and NR2F2, was significantly elevated. Additionally, tight junction (CLDN5) and gap junction (GJA4) genes were upregulated, suggesting enhanced junctional integrity. Actin polymerization related genes, such as ACTG1, CDC42BPG, RACK1, RHOG, and MYL6B, were also upregulated in co-cultured hLECs. Conversely, genes involved in endothelial adhesion with other cells or surrounding ECM, such as ITGB1, ITGA, SELE, ICAM1, and VCAM1, were downregulated. NHDF(G) co-culture also promoted the expression of endothelial mesenchymal transition (EndoMT)-related genes, including COL3A1, ACTA2, and PDGFRB, and elevated levels of ECM-degrading metalloproteinases (MMP3, MMP9, MMP2). Chemokine profiling suggested an upregulation of genes CCL21, CCL14, and CXCL14 and downregulation of CCL2, CCL20, CXCL12, CXCL8, CXCL5, and CXCL11. Gene Ontology (GO) enrichment analysis of the DEGs revealed significant alterations in key pathways related to cell adhesion and ECM remodeling, including both organization and disassembly processes. Additionally, enriched GO terms were associated

with inflammatory responses, transcriptional regulation, signal transduction pathways such as ERK1/2 and Notch, as well as angiogenesis (**Figure 6C**).

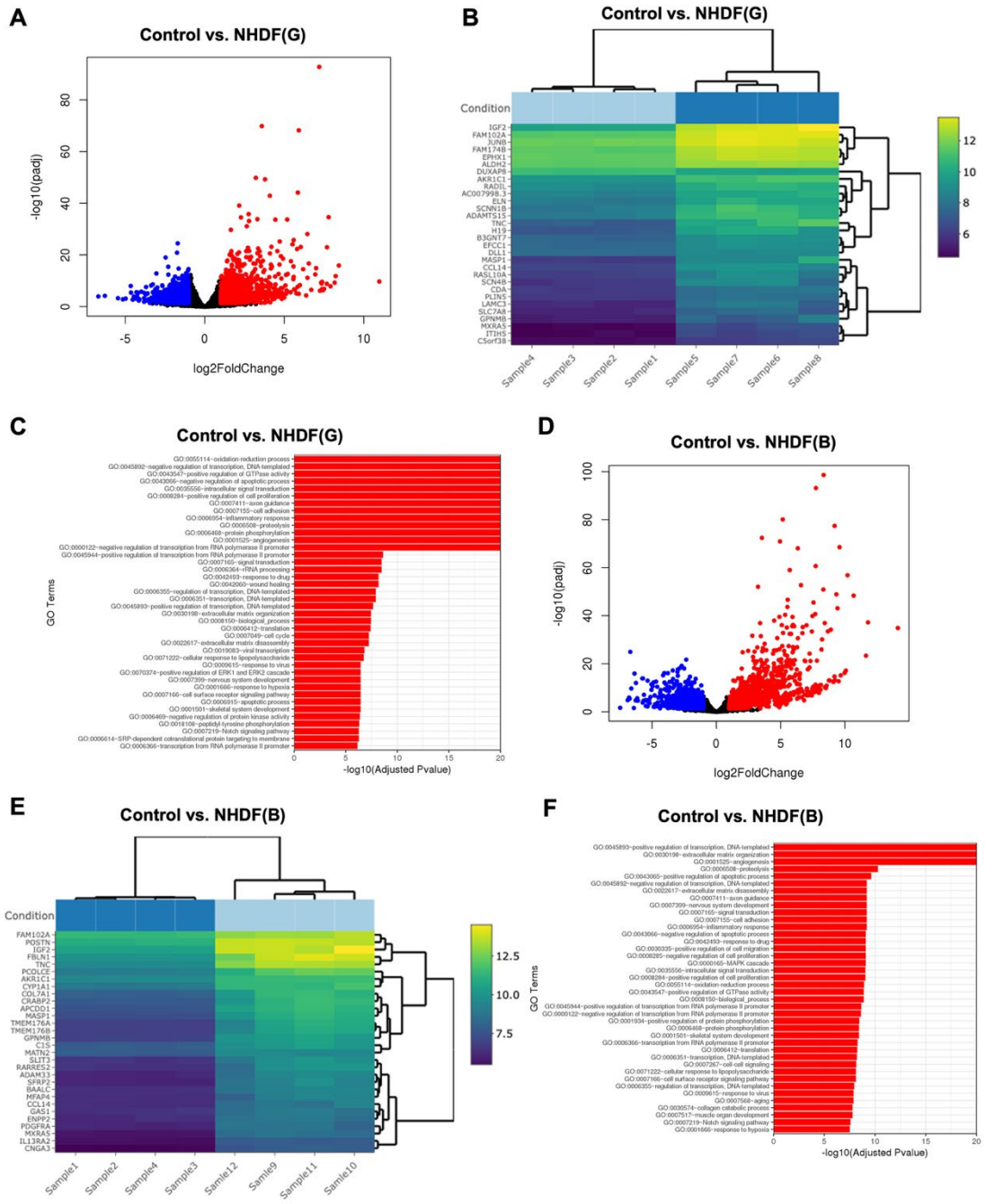

Figure 6. ***Fibroblasts regulate various cellular pathways in hLECs*****. (A)** Volcano plot of DEGs between hLEC control and hLEC co-cultured with NHDF(G). Genes with an

adjusted p-value less than 0.05 and a log2 fold change greater than 1 are indicated by red dots (upregulated genes). Genes with an adjusted p-value less than 0.05 and a log2 fold change less than -1 are indicated by green dots (downregulated genes). **(B)** A bi-clustering heatmap of top 30 DEGs sorted by their adjusted p-value between hLEC control and hLEC co-cultured with NHDF(G). **(C)** Significantly DEGs were clustered and the enrichment of gene ontology terms was tested using Fisher exact test (GeneSCF v1.1-p2) with an adjusted P-value less than 0.05. **(D)** Volcano plot of DEGs between hLEC control and hLEC co-cultured with NHDF(B). Genes with an adjusted p-value less than 0.05 and a log2 fold change greater than 1 are indicated by red dots (upregulated genes). Genes with an adjusted p-value less than 0.05 and a log2 fold change less than -1 are indicated by green dots (downregulated genes). **(E)** A bi-clustering heatmap of top 30 DEGs sorted by their adjusted p-value between hLEC control and hLEC co-cultured with NHDF(B). **(F)** Significantly DEGs were clustered and the enrichment of gene ontology terms was tested using Fisher exact test (GeneSCF v1.1-p2) with an adjusted P-value less than 0.05.

hLECs co-cultured with NHDF(B) led to the upregulation of 2,688 genes and downregulation of 1,591 genes, reflecting a largely similar transcriptomic response as observed with NHDF(G) (**Figure 6D&6E**). Similar patterns included increased expression of lymphatic markers, junctional components, actin-regulating genes, and ECM remodeling factors. However, a key distinction was the downregulation of CTNNB1 (β-catenin), a crit ical linker between cadherins and the actin cytoskeleton. Notably, hLECs co-cultured with NHDF(B) also exhibited increased expression of VEGF-C, along with VEGF-B. The NHDF(B) co-cultured hLECs also showed upregulation of EndoMT genes and mostly similar chemokine expressions consistent with the NHDF(G) condition. Another key difference is the downregulation of protease-activated receptors (PAR1, PAR2, PAR3, THBD) in NHDF(B) co-cultured hLECs, which affect thrombin-mediated vascular remodeling. The GO enrichment analysis similarly highlighted the regulation of genes involved in cell adhesion and ECM remodeling, along with associations to inflammatory responses, transcriptional regulation, and key signaling pathways including ERK1/2, Notch, and additionally, the MAPK pathway (**Figure 6F**).

A direct comparison between NHDF(B)- and NHDF(G)-induced hLECs revealed 214 genes were upregulated and 219 genes were downregulated (**Supplementary figure 2A&2B**). Moreover, ECM organization emerged as the top enriched GO term among all differentially expressed genes. The enrichment analysis also revealed consistent involvement of cellular processes related to inflammatory responses, transcriptional regulation, and key signaling pathways (**Supplementary figure 2C**).

DISCUSSION

The main objective of this study was to assess how fibroblasts regulate lymphatic permeability and barrier function. Our findings indicate that fibroblasts play a pivotal role as paracrine regulators in maintaining homeostasis by enhancing LEC junction integrity and reducing permeability in dermal lymphatic vessels. We demonstrate that the dermal fibroblast secretomes decrease lymphatic junction permeability by enhancing tight and adherens junction proteins. Our data suggest that secretome treatment increases junction integrity, as evidenced by increased TEER across LEC monolayers treated with secretome of dermal fibroblast cultures. Fibroblast secretome increased the expression of key junctional proteins (ZO-1, claudin-5, and VE-cadherin) on the hLEC surface to regulate junction morphology and paracellular transport, compared to untreated controls. We also found that treating LECs with dermal fibroblast secretome markedly reduced transport of a small, 4 kDa dextran. Finally, we found that these effects appeared to be tissue specific, as lung fibroblasts had opposite effects on hLEC integrity compared to dermal fibroblasts.

We observed that high expression of junction proteins is related to the integrity of endothelial cell monolayer. This is corroborated by others who previously demonstrated that junction localization of claudin-5 is essential for maintaining the integrity of collecting lymphatic vessels. This process is regulated by the signaling of the transmembrane ligand EphrinB2 and its receptor EphB4 [19]. Using proximity proteomics, Serafin et al. revealed changes in the VE-cadherin interactome during the transition from discontinuous to continuous LEC junctions, observing complete overlap of VE-cadherin expression in continuous cell-cell junctions [2]. Additionally, Cromer et

al. investigated the regulation of lymphatic barrier function by inflammatory cytokines, showing that inflammatory signals increase LEC permeability by reducing VE-cadherin expression [20]. Jannaway and Scallan showed a 5.7-fold increase in 3 kDa dextran transport while blocking VE-cadherin, suggesting its critical role in maintaining lymphatic barrier functions [1]. Our data also indicated a similar effect, where increased expression of VE-cadherin and ZO-1 was associated with reduced dextran transport across the monolayer. Apart from junction proteins, secretome treatment did not significantly affect LEC-specific markers such as LYVE-1 and PROX1. This suggests that LEC markers are constitutively expressed and not significantly modulated during homeostasis.

Our co-culture data corroborated the findings from secretome-treated LECs, demonstrating that fibroblasts promote continuous presentation of ZO-1 and VE-cadherin, and reduce lymphatic transport. However, lymphatic permeability is not always directly associated with changes in LEC junctional proteins. For example, a study using rat LECs reported an increase in LEC permeability and TEER induced by ethanol, despite no changes in ZO-1 or VE-cadherin expression or localization [21]. We observed similar results when examining the overall expression of junction proteins using immunoblotting and RT-qPCR analyses, which revealed no significant difference in the overall protein and mRNA expression of ZO-1 and VE-cadherin. This suggests that fibroblasts may not directly influence the translation of ZO-1 and VE-cadherin but could instead be promoting their trafficking and organization at cell-cell boundaries. Recently, Dellaquila et al., showed that HUVECs co-cultured with neonatal foreskin fibroblasts had 50% reduced permeability to 70 kDa dextrans [22]. Another study co-culturing HUVECs and lung fibroblasts showed a drop in dextran permeability for HUVECs from 61% to 39% after 7 days and to 7% after two weeks [23]. Consistent with these findings, our results also show a significant reduction in lymphatic permeability upon co-culture with dermal fibroblasts. This suggests that fibroblasts may promote remodeling of LECs towards collecting vessel phenotypes. However, further studies are needed to investigate the transition of lymphatic capillaries towards collecting vessels in the presence of fibroblasts.

Notably, LECs were either treated with secretome or introduced with fibroblasts after forming a complete LEC monolayer, highlighting the dynamic and homeostatic regulatory effect of fibroblasts on mature LECs. This is important as most of the previous studies demonstrated the role of fibroblasts in regulating LEC proliferation, lymphangiogenesis, and tube/branch formation. For instance, fibroblast-like cells have been shown to regulate the population of total endothelial cells within lymph nodes, including LECs, through paracrine signaling, primarily by secreting VEGF, which promotes cell proliferation [24]. In an in vivo study, Goto and colleagues demonstrated that interactions between LECs and surrounding fibroblasts facilitate epithelial regeneration in the small intestine [25]. Wang et al. further identified the role of specific fibroblast populations in VEGF-C-mediated lymphangiogenesis in zebrafish [10]. Additionally, Marino et al. reported that dermal fibroblasts induced lymphatic capillary branching in LECs, but only under direct contact conditions, with no branching observed when using fibroblast secretomes or a non-contact transwell setup [26]. Most of the studies discussed suggest a direct role of fibroblasts in maintaining lymphatic development and vascularization. In our studies, we also see a positive correlation between hLEC coverage and the presence of fibroblasts. However, the effect of fibroblasts in regulating LEC integrity suggests fibroblasts could be one of the key players in maintaining collecting vessels' low permeability and preventing lymphatic leakage, thus maintaining in homeostasis in the skin.

Fibroblasts are known to play a role in different tissue environments. Our data so far suggest the effect of dermal fibroblasts on maintaining dermal LEC integrity. However, unlike dermal fibroblasts, we found that lung fibroblast secretomes reduced TEER and increased FD4 transport across LEC monolayers, indicating more leaky junctions and a corresponding decline in LEC junction integrity. Surprisingly, the effect of NHLF on hLECs are opposite to what we observed with NHDF. This indicates that fibroblasts regulate LEC permeability differently depending on the tissue environment. Lung fibroblasts interact with various immune cells, influencing the severity and outcomes of many acute and chronic lung diseases, while dermal fibroblasts are key components of connective tissue, playing a role in ECM formation and wound healing. Studies have shown that dermal and pulmonary fibroblasts respond differently to TGF-β1 and PDGF-

AB, highlighting the heterogeneity of fibroblasts across different tissues [27]. Lung LECs also differ significantly from dermal LECs. Lung lymphatics are directly involved in clearing airborne toxins, gas exchange, and immune response regulation, whereas dermal LECs maintain a regular fluid homeostasis and immune surveillance within the skin layer. Lung lymphatics also lack smooth muscle coverage, unlike other collecting lymphatics, and rely on the extrinsic muscle contraction of breathing. In this study, we have also found contrary effects of lung and dermal fibroblasts on LEC permeability that might indicate tissue-specific regulation of LEC functions by fibroblasts.

Since lymphatic vessels play a key role in clearing proinflammatory mediators and immune cells to resolve inflammation, we aimed to investigate the direct impact of the inflammatory mediator thrombin on LECs in the presence of fibroblasts. A recent study reported that both human blood endothelial cells and fibroblasts can generate thrombin without the need for exogenous protein addition [28]. Previous research on dermal LECs demonstrated that thrombin reduces TEER, while pretreatment with 8-Br-cAMP mitigated this effect [29]. Additionally, researchers identified proinflammatory mediators, including thrombin, as contributors to lymphatic capillary regression [30]. Trivedi et al. used RNA sequencing of lung LECs isolated from cigarette smoke-exposed mice, which revealed an upregulation of inflammatory mediators and prothrombotic pathways. Their findings further confirmed that cigarette smoke-induced lung dysfunction is associated with increased thrombin levels [31]. While some studies suggest that thrombin compromises the lymphatic barrier, we observed minimal changes in LEC junctions upon thrombin treatment alone. However, in the presence of fibroblasts, we detected significant alterations in TEER and permeability, as indicated by increased dextran transport. Moreover, thrombin-treated LECs co-cultured with fibroblasts exhibited large gaps in the monolayer compared to control LECs. These findings suggest that fibroblasts not only influence the permeability of lymphatic endothelial junctions but also modulate the effects of other mediators on LECs.

To explore the molecular mechanisms underlying lymphatic responses to fibroblast stimulation, we performed bulk RNA sequencing and analyzed differentially expressed genes. The advent of RNA sequencing, both single-cell and bulk, has significantly advanced our understanding of lymphatic vascular biology. Recent transcriptomic

studies have uncovered the remarkable heterogeneity of LECs, revealing that these cells serve functions beyond fluid transport and immune cell trafficking - they also participate in diverse biological processes and exhibit dynamic interactions with other cell types [32, 33]. A single-cell RNA-seq study identified six distinct LEC subtypes in human lymph nodes [34], while another characterized renal LEC transcriptional responses during acute kidney injury [35]. More recently, K. C. et al. used transcriptomic profiling to show that Zmiz1-deficient LECs exhibited downregulation of genes involved in lymphatic vessel development, proliferation, and migration [36]. Moreover, RNA sequencing of recombinant and tumor cell–activated LECs revealed alterations in pathways related to endothelial activation, vascular morphogenesis, and cytokine-mediated signaling [37].

In this study, we investigated how fibroblasts influence hLECs using bulk RNA-seq. We identified 3,955 and 4,279 DEGs in hLECs co-cultured with NHDF(G) and NHDF(B) fibroblasts, respectively. Notably, in contrast to our earlier qPCR data, we observed significant upregulation of the lymphatic markers LYVE-1 and FOXC2.
Although PROX1 itself was not differentially expressed, its upstream transcriptional regulators, SOX18 and NR2F2, were significantly elevated. Consistent with our earlier findings on junctional stability, CLDN5 and GJA4 (encoding claudin-5 and gap junction A4, respectively) were also upregulated. We also observed increased expression of genes involved in actin dynamics and cytoskeletal organization, including gamma actin, RACK1, RHOG, and myosin light chain, suggesting fibroblast-induced modulation of junctional architecture. Conversely, genes associated with endothelial adhesion to neighboring cells and the extracellular matrix such as integrins, selectin E, intracellular and vascular adhesion molecules were downregulated, indicating reduced cellular and matrix interactions. A marked upregulation of matrix-degrading enzymes such as MMP3 suggested potential disruption of ECM–LEC interactions, although the concurrent increase in TIMP3 expression may reflect compensatory regulation of matrix proteolysis. Gene ontology analysis further confirmed significant enrichment in pathways related to cell–cell adhesion and ECM remodeling, involving both structural assembly and degradation processes in fibroblast-stimulated hLECs. These changes align with our observation that transport is reduced in hLECs co-cultured with NHDFs

and suggest that matrix reorganization, as well as cell-cell junction expression and reorganization, are some of the mechanisms underlying this functional outcome.

Interestingly, only NHDF(B)-induced hLECs exhibited downregulation of β-catenin, which may underlie differences in lymphatic junctional permeability between the two fibroblast co-culture conditions. Additionally, higher expression of VEGF-C in NHDF(B)-co-cultured hLECs implies an enhanced lymphatic proliferative stage compared to NHDF(G). Comparative analysis of DEGs between NHDF(B)- and NHDF(G)-induced hLECs identified 433 genes, highlighting distinct regulatory effects exerted by fibroblasts of different anatomical origins. GO enrichment in this comparison emphasized ECM remodeling as a key distinguishing feature suggesting that this may underlie the differences in endothelial permeability and junction integrity we found.

Taken together, our work explores the influence of biological and physiological factors modulating LEC barrier functions in their local microenvironment. LECs are surrounded and influenced by stromal cells and immune cells, and we demonstrate that fibroblasts play a key role in maintaining lymphatic homeostasis. Our study demonstrated that dermal fibroblasts primarily enhance LEC integrity by promoting high expression of tight and adherens proteins at cell junctions, which plays a critical role in controlling paracellular transport. Thus, fibroblasts modulate lymphatic barrier function by affecting junctional interaction, cell-cell adhesion, and ECM remodeling. However, the effect of fibroblasts on LECs showed heterogeneity and tissue specificity which warrants further investigations.

ACKNOWLEDGMENTS

Financial support was provided by the NIGMS MIRA 1R35GM142835-01(KM). We'd also like to acknowledge Michele Kaluzienski for copy-editing the finalized document, the BioWorkshop Core facility, and the Stroka Lab for helping us establish the JAnaP analysis in our lab.

MATERIALS AND METHODS

Cell culture and co-culture model

Human primary dermal lymphatic endothelial cells (hLECs) (PromoCell, C-12217) were seeded onto the bottom side of Transwell inserts (1 µm pore size, Falcon®, 353103), coated with 50 µg/mL rat tail collagen I (Corning, 354236). After seeding hLECs for 1 hour at 37 °C, inserts were turned over and cells were allowed to grow for 5 days in Endothelial Cell Growth Medium MV2 (EGM-V2; PromoCell, C-22121) until the hLECs formed a confluent monolayer. Monolayer formation was confirmed by measurement of transendothelial resistance (TEER) or by staining with CellMask™ Plasma Membrane Stain (ThermoFisher, C10046).

Normal human primary dermal fibroblasts (NHDF) were cultured in two conditions: (1) NHDF(G) (PromoCell, C-12302) in Fibroblast Growth Medium-2 (PromoCell, C-23120) containing 2% FBS, 1 ng/mL fibroblast growth factor, and 5 µg/mL insulin, or (2) NHDF(B) in fibroblast basal medium without supplements. For secretome collection, fibroblasts were cultured with EGMV2 for 24 hours. Media was then collected and centrifuged to remove debris, and the resulting conditioned medium (secretome) was used for treatment. Normal human primary lung fibroblasts (NHLF; Lonza, CC-2512) were cultured in FGM-2 (Lonza, CC-3132) and processed similarly to NHDFs for secretome collection. The hLEC monolayers on inserts were treated at the top side with either (1) NHDF cells [NHDF(G) or NHDF(B)] or (2) their corresponding secretomes, for 48 hours. Following co-culture, secretomes were removed, and fibroblasts were detached from inserts using a sterile cotton applicator (Dealmed, B074MJHSGG). hLECs were then processed for other assays. For thrombin experiments, 2 U/mL thrombin was added to the hLEC monolayer at the top. After treatment, inserts were washed thoroughly, and hLECs were co-cultured with NHDF(G) cells for 48 hours prior to downstream analysis.

Transendothelial electrical resistance (TEER)

To assess the confluence and barrier integrity of hLEC monolayers, TEER was measured using a Millicell® ERS-2 Voltohmmeter (Millipore). Electrodes were carefully positioned in both the upper and lower chambers of the Transwell system, ensuring

contact with the culture medium. Initial resistance values (in ohms) were recorded and corrected by subtracting background resistance values obtained from blank inserts (without cells). Final TEER values (Ω·cm²) were calculated by multiplying the resistance of the cell-containing inserts by the surface area of the 12-well Transwell membrane (1.12 cm²). These measurements were used to confirm monolayer confluency and LEC barrier integrity prior to downstream assays.

In vitro lymphatic transport assay

To evaluate the effect of fibroblasts or their secretomes on LEC permeability, hLEC monolayers were subjected to a transport assay following co-culture or treatment [38]. After removing fibroblasts or secretomes, hLECs were washed and incubated with fresh EGMV2 basal media. Media containing 20 µg/mL FITC-labeled dextran 4 kDa (FD4; Millipore Sigma, 46944) was added to the upper chamber of the Transwell insert. The transport assay was carried out for 8 hours at 37 °C. At defined timepoints, aliquots were collected from the lower chamber (plate bottom), and fluorescence intensity was measured using a microplate reader (Tecan Spark) and standard curve. The amount of FD4 transported across the hLEC monolayer was used as a quantitative readout of lymphatic permeability.

Immunofluorescence staining, confocal microscopy and imaging analyses

For immunofluorescence imaging and downstream analysis, hLECs were fixed in 2% paraformaldehyde (PFA) in 1X phosphate-buffered saline (PBS; Thermo Fisher, J19943.K2) for 15 minutes at room temperature, then permeabilized with 0.1% Triton X-100. Cells were blocked in 2% fetal bovine serum (FBS; Gibco, 10100-147) in PBS for 1 hour. Membranes were carefully excised and mounted onto glass slides. Cells were incubated overnight at 4°C with primary antibodies: mouse anti-VE-cadherin (1:200; BD Biosciences, 55566) and rabbit anti-ZO-1 (1:200; Invitrogen, 33-9100). The following day, cells were incubated with species-specific Alexa Fluor-conjugated secondary antibodies—donkey anti-mouse Alexa Fluor 488, 555, or 647 (1:400; Invitrogen, A21202, A31570 or A31571) and donkey anti-rabbit Alexa Fluor 488, 555, or 647 (1:400; Invitrogen, A32790, 31572 and A31573)—for 2 hours at room temperature. Washes were performed with 0.1% Tween-20 in 1X PBS (BioShop, TWN510) before

and after antibody incubations. Nuclei were counterstained using Hoechst 33342 (1:10,000) and cover slips were mounted using VECTAshield Antifade Mounting Medium with DAPI (Vector Laboratories, H-1200-10). Images were acquired using a Zeiss Observer 7 fluorescence microscope (20X/63X objectives) or an FV3000 laser scanning confocal microscope (20X/100X objectives).

Immunoblot assay and qPCR

After co-culture, hLECs were lysed using RIPA lysis buffer (Thermo Fisher, 89900). The resulting cell lysates were subjected to gel electrophoresis and immunoblotting as previously described [39]. Briefly, 20 µg of protein per lane was denatured in Laemmli buffer and separated on a 4–20% SDS-PAGE gel (Mini-Protein TGX, BioRad) at 110V for 1 hour. Proteins were then transferred to nitrocellulose membranes (Trans-Blot Turbo, BioRad) using a semi-dry transfer system (1.5 mA, 25 V for 7 minutes), and membrane transfer was confirmed via Ponceau S staining. The membranes were sectioned into strips, blocked in 2% BSA (prepared in TBS-T) for 1 hour, and incubated overnight at 4°C with primary antibodies: mouse anti-VE-cadherin (BD Biosciences, 55566) and rabbit anti-ZO-1 (Invitrogen, 33-9100) at a 1:500 dilution. After washing, the membranes were incubated for 1 hour at room temperature with secondary antibodies: IRDye® 680RD donkey anti-Rabbit, donkey anti-Mouse, and IRDye® 800CW donkey anti-Rabbit (all at 1:20,000 dilution). Protein bands were visualized using the Odyssey® Imaging System (LI-COR).

To quantify expression of genes encoding adherens and tight junction proteins, total RNA was isolated from hLEC samples using TRIzol™ reagent (Invitrogen, 15596026), following the manufacturer's protocol. To obtain sufficient RNA for analysis, biological replicates were generated by pooling RNA extracted from four individual transwell inserts. A total of 500 ng of RNA per sample was reverse transcribed into cDNA using the High-Capacity cDNA Reverse Transcription Kit (Applied Biosystems, 4374966), according to the manufacturer's instructions. Quantitative real-time PCR (RT-qPCR) was performed using TaqMan™ Gene Expression Assays specific for VE-cadherin (CDH5, Hs00901465), ZO-1 (TJP1, Hs01551871), PROX1 (Hs00896293), LYVE-1 (Hs00272659), and the housekeeping gene GAPDH (Hs02786624). Relative gene

expression levels of hLECs after co-culture were calculated using the comparative Ct method (ΔΔCt) and relative fold changes ($2^{-\Delta\Delta Ct}$) were determined with respect to control.

Image Processing

Image analysis, including cell counts and quantification of mean fluorescence intensity for junction proteins, was conducted using FIJI (ImageJ2, version 2.14). For detailed single-cell analysis, the Junction Analyzer Program (JANaP) was utilized, as previously described [17]. Junction morphology of hLECs was classified as either continuous (linear or mature) or discontinuous, which included isolated, jagged, punctate, or perpendicular junctional patterns. In addition, cell shape descriptors such as circularity and solidity were quantified to assess morphological changes.

RNA sequence analysis

Total RNA was extracted from three groups of hLECs, (1) without co-culture (control), (2) co-cultured with NHDF(G), and (3) co-cultured with NHDF(B) using TRIzol™ reagent (Invitrogen, 15596026). RNA quality was initially assessed using the NanoDrop™ 2000c spectrophotometer (Thermo Scientific). Approximately 2 µg of RNA from four biological replicates per group were sent to Genewiz, Azenta Life Sciences, for sequencing. Briefly, RNA integrity was evaluated, ensuring RIN values exceeded 9.0. RNA sequencing was performed on an Illumina platform with paired-end reads (2×150 bp), generating approximately 50 million reads per sample.

In the bioinformatics pipeline, raw reads were trimmed using Trimmomatic v0.36, and then aligned to the GRCh38 human reference genome using STAR aligner v2.5.2b. Gene hit counts were calculated using the Subread package v1.5.2 and subsequently normalized. Differentially expressed genes (DEGs) were identified using DESeq2, with p-values and $\log_2$ fold changes calculated via the Wald test. Genes with an adjusted p-value < 0.05 and an absolute $\log_2$ fold change > 1 were considered significantly differentially expressed. The top 30 DEGs, ranked by adjusted p-value, were visualized in a bi-clustered heatmap. A volcano plot was generated to depict the overall distribution of up- and downregulated genes. Gene Ontology (GO) enrichment analysis of the

significant DEGs was conducted using GeneSCF v1.1-p2 with the *goa_human* annotation list.

Statistical Analysis

All analysis was performed using GraphPad software (version 10.4.2), and data are represented as mean ± standard error of the mean (SEM). Statistical analysis was performed using an unpaired two-tailed *t*-test; $p > 0.05$ = not significant (ns), $p \leq 0.0001$ = extremely significant (****). For the permeability (transport) assay, statistical significance was determined by two-way ANOVA followed by appropriate post hoc test for multiple comparisons.

FIGURE LEGENDS:

Figure 1. ***NHDF secretomes increase hLEC barrier functions.*** **(A)** Schematic diagram of transwell secretome experiment. (**B)** TEER measurements of hLEC monolayers after 48 hours of treatment with dermal fibroblast secretomes from NHDF(G) and NHDF(B). (**C)** Representative immunofluorescence images of VE-cadherin, claudin-5, and ZO-1 on hLECs following treatment with NHDF secretomes. **(D)** Quantification of VE-cadherin, claudin-5, and ZO-1 expression levels using ImageJ (FIJI). **(E)** Quantification of lymphatic markers LYVE-1 and PROX1 expression in hLEC monolayers treated with NHDF secretomes. **(F)** FITC–Dextran (4 kDa) transport assay across hLECs after NHDF secretome treatment. Data are presented as mean ± SEM from n = 6 independent experiments. Statistical analysis was performed using an unpaired two-tailed t-test; $p > 0.05$ = not significant (ns), $p \leq 0.0001$ = extremely significant (****). For the permeability (transport) assay (n = 3, representative), statistical significance was determined by two-way ANOVA followed by appropriate post hoc test for multiple comparisons.

Figure 2. ***NHDF co-culture with hLECs increases hLEC barrier functions.*** **(A)** Schematic diagram of transwell co-culture experiment and timeline of cell seedings and co-culture. **(B)** TEER measurements of hLEC monolayers after 48 hours of co-culture with dermal fibroblasts, NHDF(G) and NHDF(B). **(C)** Representative immunofluorescence images of VE-cadherin, and ZO-1 on hLECs following co-culture with NHDFs. **(D)** Quantification of VE-cadherin and ZO-1 expression levels using ImageJ (FIJI). **(E)** FITC–Dextran (4 kDa) transport assay across hLECs after co-culture with NHDFs. Data are presented as mean ± SEM from n = 6 independent experiments. Statistical analysis was performed using an unpaired two-tailed t-test; $p > 0.05$ = not significant (ns), $p \leq 0.0001$ = extremely significant (****). For the permeability (transport) assay (n = 9, representative), statistical significance was determined by two-way ANOVA followed by appropriate post hoc test for multiple comparisons.

Figure 3. ***hLEC junctions are tightened after co-culture with NHDFs.*** **(A)** Quantitative analysis of ZO-1 distribution and organization in hLEC monolayers using JAnaP after 48 hours of co-culture with NHDFs. **(B)** Immunoblot analysis of total ZO-1

(220 kDa) and VE-cadherin (120 kDa) protein expression levels in hLECs following co-culture. **(C)** RT-qPCR analysis of mRNA expression levels of ZO-1 and VE-cadherin in hLECs under the same conditions. Data are presented as mean ± SEM from $n > 2$ independent experiments. Statistical analysis was performed using an unpaired two-tailed *t*-test; $p > 0.05$ = not significant (ns), $p \leq 0.0001$ = extremely significant (****).

Figure 4. ***NHLF secretomes reduce hLEC barrier functions.*** **(A)** TEER measurements of hLEC monolayers after 48 hours of treatment with NHLF secretomes or fibroblast media. **(B)** Representative immunofluorescence images of VE-cadherin, and ZO-1 on hLECs following treatment with NHLF secretome. **(C)** Quantification of VE-cadherin and ZO-1 expression levels using ImageJ (FIJI). **(D)** FITC–Dextran (4 kDa) transport assay across hLECs after treatment with 10, 25, and 50% NHLF secretome. Data are presented as mean ± SEM from $n = 6$ independent experiments. Statistical analysis was performed using an unpaired two-tailed *t*-test; $p > 0.05$ = not significant (ns), $p \leq 0.0001$ = extremely significant (****). For the transport assay ($n = 3$, representative), statistical significance was determined by two-way ANOVA followed by appropriate post hoc test for multiple comparisons.

Figure 5. ***Thrombin modulates hLEC barrier integrity only in the context of co-culture with NHDFs.*** **(A)** TEER measurements of hLEC monolayers after 4 hours of thrombin treatment followed by 48 hours of co-culture with dermal fibroblast, NHDF(G) ($n = 3$). **(B)** Total cell counts ($n = 6$). **(C)** FITC–Dextran (4 kDa) transport assay across hLECs after 4 hours of thrombin stimulation and/or NHDF(G) co-culture for 48 hours. **(D)** Representative immunofluorescence images of ZO-1 and VE-cadherin on hLECs with and without thrombin treatment. Data are presented as mean ± SEM from $n = 3\text{-}6$ independent experiments. Statistical analysis was performed using an unpaired two-tailed *t*-test; $p > 0.05$ = not significant (ns), $p \leq 0.0001$ = extremely significant (****). For the transport assay, statistical significance was determined by two-way ANOVA followed by appropriate post hoc test for multiple comparisons.

Figure 6. ***Fibroblasts regulate various cellular pathways in hLECs*****. (A)** Volcano plot of DEGs between hLEC control and hLEC co-cultured with NHDF(G). Genes with an adjusted p-value less than 0.05 and a log2 fold change greater than 1 are indicated by

red dots (upregulated genes). Genes with an adjusted p-value less than 0.05 and a log2 fold change less than -1 are indicated by green dots (downregulated genes). **(B)** A bi-clustering heatmap of top 30 DEGs sorted by their adjusted p-value between hLEC control and hLEC co-cultured with NHDF(G). **(C)** Significantly DEGs were clustered and the enrichment of gene ontology terms was tested using Fisher exact test (GeneSCF v1.1-p2) with an adjusted P-value less than 0.05. **(D)** Volcano plot of DEGs between hLEC control and hLEC co-cultured with NHDF(B). Genes with an adjusted p-value less than 0.05 and a log2 fold change greater than 1 are indicated by red dots (upregulated genes). Genes with an adjusted p-value less than 0.05 and a log2 fold change less than -1 are indicated by green dots (downregulated genes). **(E)** A bi-clustering heatmap of top 30 DEGs sorted by their adjusted p-value between hLEC control and hLEC co-cultured with NHDF(B). **(F)** Significantly DEGs were clustered and the enrichment of gene ontology terms was tested using Fisher exact test (GeneSCF v1.1-p2) with an adjusted P-value less than 0.05.

Supplementary Figure 1. (A) Representative immunofluorescence images of PROX1 and LYVE-1 on hLECs following treatment with NHDF secretomes. (**B**) RT-qPCR analysis of mRNA expression levels of PROX1 and LYVE-1 in hLECs following NHDFs co-culture.

Supplementary Figure 2. (A) Volcano plot of DEGs between hLECs co-cultured with NHDF(G) and NHDF(B). Genes with an adjusted p-value less than 0.05 and a log2 fold change greater than 1 are indicated by red dots (upregulated genes). Genes with an adjusted p-value less than 0.05 and a log2 fold change less than -1 are indicated by green dots (downregulated genes). **(B)** A bi-clustering heatmap of top 30 DEGs sorted by their adjusted p-value between hLECs co-cultured with NHDF(G) and NHDF(B). **(C)** Significantly DEGs were clustered and the enrichment of gene ontology terms was tested using Fisher exact test (GeneSCF v1.1-p2) with an adjusted P-value less than 0.05.

References

1. Jannaway, M., & Scallan, J. P. (2021). VE-Cadherin and Vesicles Differentially Regulate Lymphatic Vascular Permeability to Solutes of Various Sizes. Frontiers in physiology, 12, 687563. https://doi.org/10.3389/fphys.2021.687563

2. Serafin, D. S., Harris, N. R., Bálint, L., Douglas, E. S., & Caron, K. M. (2024). Proximity interactome of lymphatic VE-cadherin reveals mechanisms of junctional remodeling and reelin secretion. *Nature communications*, *15*(1), 7734. https://doi.org/10.1038/s41467-024-51918-1

3. Peluzzo, A. M., Bkhache, M., Do, L. N. H., Autieri, M. V., & Liu, X. (2023). Differential regulation of lymphatic junctional morphology and the potential effects on cardiovascular diseases. Frontiers in physiology, 14, 1198052. https://doi.org/10.3389/fphys.2023.1198052

3. Kajiya, K., Kidoya, H., Sawane, M., Matsumoto-Okazaki, Y., Yamanishi, H., Furuse, M., & Takakura, N. (2012). Promotion of lymphatic integrity by angiopoietin-1/Tie2 signaling during inflammation. The American journal of pathology, 180(3), 1273–1282. https://doi.org/10.1016/j.ajpath.2011.11.008

5. Miteva, D. O., Rutkowski, J. M., Dixon, J. B., Kilarski, W., Shields, J. D., & Swartz, M. A. (2010). Transmural flow modulates cell and fluid transport functions of lymphatic endothelium. *Circulation research*, *106*(5), 920–931. https://doi.org/10.1161/CIRCRESAHA.109.207274

6. Ilan, I. S., Yslas, A. R., Peng, Y., Lu, R., & Lee, E. (2023). A 3D Human Lymphatic Vessel-on-Chip Reveals the Roles of Interstitial Flow and VEGF-A/C for Lymphatic Sprouting and Discontinuous Junction Formation. *Cellular and molecular bioengineering*, *16*(4), 325–339. https://doi.org/10.1007/s12195-023-00780-0

7. Frye, M., Taddei, A., Dierkes, C., Martinez-Corral, I., Fielden, M., Ortsäter, H., Kazenwadel, J., Calado, D. P., Ostergaard, P., Salminen, M., He, L., Harvey, N. L., Kiefer, F., & Mäkinen, T. (2018). Matrix stiffness controls lymphatic vessel formation through regulation of a GATA2-dependent transcriptional program. Nature communications, 9(1), 1511.

8. Norden, P. R., & Kume, T. (2021). Molecular Mechanisms Controlling Lymphatic Endothelial Junction Integrity. *Frontiers in cell and developmental biology*, *8*, 627647. https://doi.org/10.3389/fcell.2020.627647

9. Hong, S. P., Yang, M. J., Cho, H., Park, I., Bae, H., Choe, K., Suh, S. H., Adams, R. H., Alitalo, K., Lim, D., & Koh, G. Y. (2020). Distinct fibroblast subsets regulate lacteal integrity through YAP/TAZ-induced VEGF-C in intestinal villi. *Nature communications*, *11*(1), 4102. https://doi.org/10.1038/s41467-020-17886-y

10. Wang, G., Muhl, L., Padberg, Y., Dupont, L., Peterson-Maduro, J., Stehling, M., le Noble, F., Colige, A., Betsholtz, C., Schulte-Merker, S., & van Impel, A. (2020). Specific fibroblast subpopulations and neuronal structures provide local sources of Vegfc-processing components during zebrafish lymphangiogenesis. *Nature communications*, *11*(1), 2724. https://doi.org/10.1038/s41467-020-16552-7

11. Karkkainen, M. J., Haiko, P., Sainio, K., Partanen, J., Taipale, J., Petrova, T. V., Jeltsch, M., Jackson, D. G., Talikka, M., Rauvala, H., Betsholtz, C., & Alitalo, K. (2004). Vascular endothelial growth factor C is required for sprouting of the first lymphatic vessels from embryonic veins. Nature immunology, 5(1), 74–80. https://doi.org/10.1038/ni1013

12. Lee, E., Chan, S. L., Lee, Y., Polacheck, W. J., Kwak, S., Wen, A., Nguyen, D. T., Kutys, M. L., Alimperti, S., Kolarzyk, A. M., Kwak, T. J., Eyckmans, J., Bielenberg, D. R., Chen, H., & Chen, C. S. (2023). A 3D biomimetic model of lymphatics reveals cell-cell junction tightening and lymphedema via a cytokine-induced ROCK2/JAM-A complex. Proceedings of the National Academy of Sciences of the United States of America, 120(41), e2308941120. https://doi.org/10.1073/pnas.2308941120

13. Yu, P., Wilhelm, K., Dubrac, A., Tung, J. K., Alves, T. C., Fang, J. S., Xie, Y., Zhu, J., Chen, Z., De Smet, F., Zhang, J., Jin, S. W., Sun, L., Sun, H., Kibbey, R. G., Hirschi, K. K., Hay, N., Carmeliet, P., Chittenden, T. W., Eichmann, A., … Simons, M. (2017). FGF-dependent metabolic control of vascular development. Nature, 545(7653), 224–228. https://doi.org/10.1038/nature22322

14. Wei, W. F., Zhou, H. L., Chen, P. Y., Huang, X. L., Huang, L., Liang, L. J., Guo, C. H., Zhou, C. F., Yu, L., Fan, L. S., & Wang, W. (2023). Cancer-associated fibroblast-derived PAI-1 promotes lymphatic metastasis via the induction of EndoMT in lymphatic endothelial cells. Journal of experimental & clinical cancer research : CR, 42(1), 160. https://doi.org/10.1186/s13046-023-02714-0

15. Lugo-Cintrón, K. M., Ayuso, J. M., Humayun, M., Gong, M. M., Kerr, S. C., Ponik, S. M., Harari, P. M., Virumbrales-Muñoz, M., & Beebe, D. J. (2021). Primary head and neck tumour-derived fibroblasts promote lymphangiogenesis in a lymphatic organotypic co-culture model. *EBioMedicine*, *73*, 103634. https://doi.org/10.1016/j.ebiom.2021.103634

16. Chiu, A., Jia, W., Sun, Y., Goldman, J., & Zhao, F. (2023). Fibroblast-Generated Extracellular Matrix Guides Anastomosis during Wound Healing in an Engineered Lymphatic Skin Flap. *Bioengineering (Basel, Switzerland)*, *10*(2), 149. https://doi.org/10.3390/bioengineering10020149

17. Gray, K. M., Katz, D. B., Brown, E. G., & Stroka, K. M. (2019). Quantitative Phenotyping of Cell-Cell Junctions to Evaluate ZO-1 Presentation in Brain Endothelial Cells. *Annals of biomedical engineering*, *47*(7), 1675–1687. https://doi.org/10.1007/s10439-019-02266-5

18. Rabiet, M. J., Plantier, J. L., Rival, Y., Genoux, Y., Lampugnani, M. G., & Dejana, E. (1996). Thrombin-induced increase in endothelial permeability is associated with changes in cell-to-cell junction organization. *Arteriosclerosis, thrombosis, and vascular biology*, *16*(3), 488–496. https://doi.org/10.1161/01.atv.16.3.488

19. Frye, M., Stritt, S., Ortsäter, H., Hernandez Vasquez, M., Kaakinen, M., Vicente, A., Wiseman, J., Eklund, L., Martínez-Torrecuadrada, J. L., Vestweber, D., & Mäkinen, T. (2020). EphrinB2-EphB4 signalling provides Rho-mediated homeostatic control of lymphatic endothelial cell junction integrity. eLife, 9, e57732. https://doi.org/10.7554/eLife.57732

20. Cromer, W. E., Zawieja, S. D., Tharakan, B., Childs, E. W., Newell, M. K., & Zawieja, D. C. (2014). The effects of inflammatory cytokines on lymphatic endothelial barrier function. Angiogenesis, 17(2), 395–406. https://doi.org/10.1007/s10456-013-9393-2

21. Herrera, M., Molina, P., & Souza-Smith, F. M. (2021). Ethanol-induced lymphatic endothelial cell permeability via MAP-kinase regulation. American journal of physiology. Cell physiology, 321(1), C104–C116. https://doi.org/10.1152/ajpcell.00039.2021

22. Dellaquila, A., Dujardin, C., Le Bao, C., Chaumeton, C., Carré, A., Le Guilcher, C., Lam, F., & Simon-Yarza, T. (2023). Fibroblasts mediate endothelium response to angiogenic cues in a newly developed 3D stroma engineered model. Biomaterials advances, 154, 213636. https://doi.org/10.1016/j.bioadv.2023.213636

23. Grainger, S. J., & Putnam, A. J. (2011). Assessing the permeability of engineered capillary networks in a 3D culture. PloS one, 6(7), e22086. https://doi.org/10.1371/journal.pone.0022086

24. Chyou, S., Ekland, E. H., Carpenter, A. C., Tzeng, T. C., Tian, S., Michaud, M., Madri, J. A., & Lu, T. T. (2008). Fibroblast-type reticular stromal cells regulate the lymph node vasculature. Journal of immunology (Baltimore, Md. : 1950), 181(6), 3887–3896. https://doi.org/10.4049/jimmunol.181.6.3887

25. Goto, N., Goto, S., Imada, S., Hosseini, S., Deshpande, V., & Yilmaz, Ö. H. (2022). Lymphatics and fibroblasts support intestinal stem cells in homeostasis and injury. Cell stem cell, 29(8), 1246–1261.e6. https://doi.org/10.1016/j.stem.2022.06.013

26. Marino, D., Luginbühl, J., Scola, S., Meuli, M., & Reichmann, E. (2014). Bioengineering dermo-epidermal skin grafts with blood and lymphatic capillaries. Science translational medicine, 6(221), 221ra14. https://doi.org/10.1126/scitranslmed.3006894

27. Madsen, S. F., Sand, J. M. B., Juhl, P., Karsdal, M., Thudium, C. S., Siebuhr, A. S., & Bay-Jensen, A. C. (2023). Fibroblasts are not just fibroblasts: clear differences

between dermal and pulmonary fibroblasts' response to fibrotic growth factors. Scientific reports, 13(1), 9411. https://doi.org/10.1038/s41598-023-36416-6

28. Cohen, C. T., Turner, N. A., & Moake, J. L. (2021). Human endothelial cells and fibroblasts express and produce the coagulation proteins necessary for thrombin generation. *Scientific reports*, *11*(1), 21852. https://doi.org/10.1038/s41598-021-01360-w

29. Breslin J. W. (2011). ROCK and cAMP promote lymphatic endothelial cell barrier integrity and modulate histamine and thrombin-induced barrier dysfunction. *Lymphatic research and biology*, *9*(1), 3–11. https://doi.org/10.1089/lrb.2010.0016

30. Kemp, S. S., Penn, M. R., Koller, G. M., Griffin, C. T., & Davis, G. E. (2022). Proinflammatory mediators, TNFα, IFNγ, and thrombin, directly induce lymphatic capillary tube regression. *Frontiers in cell and developmental biology*, *10*, 937982. https://doi.org/10.3389/fcell.2022.937982

31. Trivedi, A., Lu, T. M., Summers, B., Kim, K., Rhee, A. J., Houghton, S., Byers, D. E., Lis, R., & Reed, H. O. (2024). Lung lymphatic endothelial cells undergo inflammatory and prothrombotic changes in a model of chronic obstructive pulmonary disease. *Frontiers in cell and developmental biology*, *12*, 1344070. https://doi.org/10.3389/fcell.2024.1344070

32. Miyasaka M. (2021). A short review on lymphatic endothelial cell heterogeneity. *Inflammation and regeneration*, *41*(1), 32. https://doi.org/10.1186/s41232-021-00183-6

33. den Braanker, H., van Stigt, A. C., Kok, M. R., Lubberts, E., & Bisoendial, R. J. (2021). Single-Cell RNA Sequencing Reveals Heterogeneity and Functional Diversity of Lymphatic Endothelial Cells. *International journal of molecular sciences*, *22*(21), 11976. https://doi.org/10.3390/ijms222111976

34. Takeda, A., Hollmén, M., Dermadi, D., Pan, J., Brulois, K. F., Kaukonen, R., Lönnberg, T., Boström, P., Koskivuo, I., Irjala, H., Miyasaka, M., Salmi, M., Butcher, E. C., & Jalkanen, S. (2019). Single-Cell Survey of Human Lymphatics Unveils

Marked Endothelial Cell Heterogeneity and Mechanisms of Homing for Neutrophils. *Immunity*, *51*(3), 561–572.e5. https://doi.org/10.1016/j.immuni.2019.06.027

35. Creed, H. A., Kannan, S., Tate, B. L., Godefroy, D., Banerjee, P., Mitchell, B. M., Brakenhielm, E., Chakraborty, S., & Rutkowski, J. M. (2024). Single-Cell RNA Sequencing Identifies Response of Renal Lymphatic Endothelial Cells to Acute Kidney Injury. *Journal of the American Society of Nephrology : JASN*, *35*(5), 549–565. https://doi.org/10.1681/ASN.0000000000000325

36. K C, R., Patel, N. R., Shenoy, A., Scallan, J. P., Chiang, M. Y., Galazo, M. J., & Meadows, S. M. (2024). Zmiz1 is a novel regulator of lymphatic endothelial cell gene expression and function. PloS one, 19(5), e0302926. https://doi.org/10.1371/journal.pone.0302926

37. Turati, M., Mattei, G., Boaretto, A., Magi, A., Calvani, M., & Ronca, R. (2023). Molecular Profiling of Lymphatic Endothelial Cell Activation In Vitro. *International journal of molecular sciences*, *24*(23), 16587. https://doi.org/10.3390/ijms242316587

38. McCright, J., Skeen, C., Yarmovsky, J., & Maisel, K. (2022). Nanoparticles with dense poly(ethylene glycol) coatings with near neutral charge are maximally transported across lymphatics and to the lymph nodes. *Acta biomaterialia*, *145*, 146–158. https://doi.org/10.1016/j.actbio.2022.03.054

39. Ejazi, S. A., Bhattacharyya, A., Choudhury, S. T., Ghosh, S., Sabur, A., Pandey, K., Das, V. N. R., Das, P., Rahaman, M., Goswami, R. P., & Ali, N. (2018). Immunoproteomic Identification and Characterization of Leishmania Membrane Proteins as Non-Invasive Diagnostic Candidates for Clinical Visceral Leishmaniasis. *Scientific reports*, *8*(1), 12110. https://doi.org/10.1038/s41598-018-30546-y